Nano Hybrids *Online: 2012-05-14*
ISSN: 2234-9871, Vol. 1, pp 57-80
doi:10.4028/www.scientific.net/NH.1.57

Correlation of surface properties and photocatalytic activity of nanocrystalline TiO_2 on the synthesis route

Manoj A. Lazar, Rajesh J. Tayade, H. C. Bajaj and R. V. Jasra[*#]

Discipline of Inorganic Materials and Catalysis, Central Salt and Marine Chemicals Research Institute (CSMCRI), Council of Scientific & Industrial Research (CSIR), G. B. Marg, Bhavnagar, Gujarat 364002, India.

*To whom correspondence should be addressed. Fax: +91 0265-6693934; Tel.: +91 0265 669 6313 / 669 3935; E-mail: rvjasra@gmail.com; rakshvir.jasra@ril.com

[#] Present address*:* R&D Centre, VMD, Reliance Industries Limited, Vadodara – 391 346, Gujarat, India.

Keywords: semiconductors, chemical synthesis; chemical techniques; nitro aromatic pollutants, degradation.

Abstract. Present work describes the synthesis of nanocrystalline TiO_2 photocatalyst using sol-gel and solution combustion methods and their characterisation by powder X-ray Diffraction, Diffuse Reflectance Spectroscopy, surface area measurement, FT-IR, FT-Raman, Thermo Gravimetric Analysis, and Transmission Electron Microscopy. Their photocatalytic activity was evaluated by the degradation of two nitro aromatic pollutants, viz. para-nitroaniline (PNA) & meta-dinitrobenzoic acid (DNBA) commonly observed in nitroaromatic plants. Performance of the synthesized catalysts was compared with commercial Degussa P25 sample. The photocatalytic degradation and total mineralization were monitored using UV/VIS spectrophotometer and total organic carbon content analysis respectively. The materials properties such as crystallinity and surface hydroxyl group on the nanocrystalline TiO_2 played crucial role for the total mineralization of the nitroaromatics.

Introduction

Subsequent to reporting of photocatalytic splitting of water on a TiO_2 electrode under ultraviolet (UV) light [1], a vast area of semiconductor mediated photocatalytic processes has opened. Among the various semiconductors, TiO_2 is widely studied for photocatalytic and other applications such as photovoltaics, photo-/ electrochromics and sensors [2]. Photocatalytic decomposition of pollutants is one of the prime applications of TiO_2 and is potentially used as the most efficient and eco-friendly process. Semiconductor sensitized oxidative mineralization of organic pollutant was first reported by Ollis and coworkers [3,4] for the mineralization of halogenated hydrocarbons, including trichloroethylene, dichloromethane, chloroform and carbon tetrachloride. The photocatalytic activity of a semiconductor is mainly determined [5] by (i) the light absorption properties, (ii) oxidation and reduction rates on the surface by the hole and electron, and (iii) the electron-hole recombination rate. Higher photocatalytic reaction rates can be achieved on the surfaces with large surface area and constant surface density of adsorbents. However, with surface being defect site, the rate of recombination of the electron-hole pair will increases with increase in surface area [6]. Surface with minimum bulk defects (higher crystallinity) is obtainable by high temperature treatment. However, this in turn, can induce the aggregation of small nanoparticles thereby decreasing the surface area. Hence, the relation between the structural & textural properties of the semiconductor and the photocatalytic activities is to be understood for determining an optimum photocatalyst. The physical and photochemical characteristics such as morphology, crystal phase, specific surface area, particle aggregate size and surface density of OH groups in the TiO_2 appear to be highly dependent on the exact experimental conditions used during synthesis. Among the various methods [2] used for preparation nanocrystalline TiO_2, sol-gel route is a simple and versatile process for the synthesis of nanocrystalline materials. The solution combustion method is a single-step process that results into fine particles and large surface area oxide materials.

Present work describes synthesis of nanocrystalline TiO_2 using sol-gel [7] as well as solution combustion methods [8]. In a typical sol-gel process, the hydrolysis and polymerization reactions of the precursors, generally inorganic metal salts or metal organic compounds, such as metal alkoxide, leads to a formation of a suspension or a sol and complete polymerization and loss of solvent leads to the transition from the liquid sol into a solid gel phase [9-11]. Low content of water, low hydrolysis rates, and excess titanium alkoxide in the reaction mixture will lead to the formation of three dimensional polymeric skeletons with close packing that result from the development of Ti-O-Ti chains. With high hydrolysis rates for an average amount of water the formation of $Ti(OH)_4$ is favored [12]. In solution combustion method, an aqueous redox mixture containing stoichiometric amounts of metal salts and water-soluble fuel is heated rapidly. Nano-TiO_2 with higher dispersing ability, in water, with easy separation of the catalyst by centrifugation has been reported using this method [13,14].

Different characterization techniques were used to study the surface properties of the nanocrystalline TiO_2 obtained by these two methods. Their photocatalytic activity was evaluated for the degradation of nitro aromatic compounds. We have tried to correlate the surface properties of the two synthesized catalysts with their obtained photocatalytic activities. A comparative study of the synthesized TiO_2 catalysts with standard Degussa P25 sample, for their photocatalytic activity, has also been carried out. The selected nitro aromatic compounds for the degradation studies are *p*-nitroaniline (PNA) and *m*-dinitrobenzoic acid (DNBA) which are commonly employed in the production of dyes and explosives. Nitro-aromatic compounds, in general, are toxic in nature, resistant to degradation and may act as an inhibitor for the biodegradation of other compounds in the waste materials [15]. DNBA is commonly found in the vicinity of ammunition plants and it's presence in ground- and drinking water is of great environmental concern. Identification of DNBA, from polar metabolites of explosives, and its fragmentation behaviour has been reported [16,17]. Toxicity of PNA in human body and its metabolites have identified and have reported from a death

case that happened after oral p-nitroaniline intake which occurred in Berlin in 2005 [18]. Photocatalytic as well as photolytic degradation of PNA has been reported by different research groups [19,20].

Experimental

Chemicals & Materials. Titanium dioxide, P25, was purchased from Degussa AG, Frankfurt, Germany. Titanium (IV) tetraisopropoxide, 97 % (Sigma Aldrich India), Glycine (Qualigens, India) and nitric acid AR (RANKEM, India) were used as such for the synthesis of the catalysts. *P*-nitroaniline (PNA) and *m*-dinitrobenzoicacid (DNBA) were purchased from Merck, India. De-ionized distilled water was used for the catalyst synthesis, photo catalytic reactions and the analysis purposes.

Preparation of the Catalysts. 38 ml of titanium (IV) tetraisopropoxide in 120 ml of dry ethanol was taken in a 500 ml round bottom flask and stirred (ca. 950 rpm) for around 30 minutes for the sol-gel synthesis. Around 160 ml of distilled water was added drop by drop into this mixture to hydrolyze titanium (IV) tetra-isopropoxide. The resulting slurry was peptized for 12 hours. The solvent from the slurry was slowly removed by rotavapor (*Buchi Rotavapor R-205*) at 343 K and the sample obtained was calcined in presence of air at 723 K for 4 hours with a heating rate of 5˚C min^{-1}. The catalyst thus obtained was named as SG.

In solution combustion synthesis, a Pyrex dish containing an aqueous redox mixture of stoichiometric amounts of titanylnitrate (2.5 g) and glycine (1.11 g) in 20 mL of distilled water was introduced in to a muffle furnace preheated to 623 K. Titanylnitrate was obtained by adding concentrated HNO_3 to titanium hydroxide, made by sol–gel method, with stirring and re-precipitated by adding acetone. Inside the furnace, the solution initially undergoes dehydration and a spark appears at one corner which spreads throughout the mass, yielding predominantly anatase titania. This sample was then calcined at 723 K at a heating rate of 5 °C min^{-1} under air flow. The catalyst thus obtained was named as SC.

Catalyst Characterization. Powder X-ray diffraction patterns of the samples were recorded using Cu Kα1 (λ = 0.15405 nm) radiation at room temperature with Phillips X'pert MPD system over the 2θ range of 10°- 70° at the scan speed of 0.1°sec^{-1}. The XRD peaks at 2θ = 25.3°, 27.4° and at 30.7° corresponds to the diffraction from the (101) crystal plane of anatase phase, (110) crystal plane of rutile phase and the (121) crystal plane of brookite phase respectively [21,22]. The phase content of a sample has been calculated from the integrated intensities of anatase (101), rutile (110), and brookite (121) peaks using the following equations:

$$W_A = \frac{K_A A_A}{K_A A_A + A_R + K_B A_B} \tag{1a}$$

$$W_R = \frac{A_R}{K_A A_A + A_R + K_B A_B} \tag{1b}$$

$$W_B = \frac{K_B A_B}{K_A A_A + A_R + K_B A_B} \tag{1c}$$

Where, W_A and W_B represent the mass fractions of anatase and brookite, respectively. A_B is the integrated intensity of the brookite (121) peak, and K_A and K_B are two coefficients with values of 0.886 and 2.721 respectively. The anatase crystallite size of the catalysts was determined from the characteristic peak at 2θ = 25.3 for the (101) plane of the anatase phase using the Scherer formula [23], with a shape factor (K) of 0.9 as follows:

$$\text{Crystallite size} = K\lambda / W \cos\theta, \tag{2}$$

Where, $W = W_b - W_s$, W_b is the broadened profile width of experimental sample. Ws is the standard profile width of reference silicon sample, λ is the wavelength of X-ray radiation. The crystallinity of the catalysts was calculated with reference to P25 Degussa by taking the average of the five major anatase peaks of the catalyst (2θ = 25.3, 37.7, 47.9, 53.9 and 55.2).

The Brunauer-Emmett-Teller (BET) surface areas [24] of the powders were determined from the nitrogen adsorption isotherm measured at 77.4 K using a volumetric adsorption set-up (Micromeritics ASAP 2010). Catalyst samples were degassed at 350 °C for 2 h under a vacuum of 5 x 10^{-5} mm Hg prior to N_2 adsorption measurement. FT-IR analysis was carried out on a Perkin-Elmer GX spectrophotometer. The samples were incorporated in KBr pellets for the measurements. The spectra were recorded in the range of 400-4000 cm^{-1} with a resolution of 4 cm^{-1}. FT-Raman spectra were recorded with Thermo Electron Corporation (Nicolet 6700) spectrophotometer. The Diffuse Reflectance Spectra were taken at room temperature in the range of 250-650 nm using Shimadzu UV-3101PC spectrophotometer equipped with an integrity sphere and $BaSO_4$ was used as the reference material. The bandgap energies of the catalysts were calculated according to the equation,

$$\text{Bandgap } (E_g) = hc/\lambda. \quad (3)$$

where h is the plank's constant, c is the velocity of the light and λ is the wavelength of the adsorbed radiation.

The morphology of the synthesized catalysts was determined using Transmission Electron Microscopy, TEM, (JEOL, JEM-2100). Thermo Gravimetric Analysis (TGA) was done using Mettler Toledo Star^e SW 7.01 TG analyzer. Temperature-programmed desorption of ammonia (NH_3-TPD) was carried out on a Micromeritics TPR/TPD 2900 apparatus equipped with a thermal conductivity detector (TCD). Approximately 25 mg of sample was pretreated at 125 °C and rapidly cooled to 100 °C and loaded with ammonia applying a flow of 30 mL min^{-1} for about 1 h. A helium flow of 30 mL min^{-1} was applied to remove weakly adsorbed NH_3. A linear temperature program was started (100-800 °C at 10 K min-1) and the desorbed amount of ammonia was analyzed by TCD. The TPD spectra were used to analyze the concentration of OH- groups (OH) present on the surface of the catalyst sample.

Photocatalytic Activity. Photocatalytic degradation of *p*- nitroaniline and *m*- dinitrobenzoic acid was carried out using a locally fabricated reactor consisting of two parts [25]. The first part is a double wall quartz vessel having an empty chamber at the centre to immerse the irradiation source. This quartz jacket has an inlet and an outlet meant for water circulation by which the temperature can be maintained throughout the reaction. The UV irradiation source used [26] was a 125W mercury vapour lamp (Crompton, radiation wavelength 280–450 nm). The second outer part consists of a borosilicate glass container in which the quartz jacket is inserted. The solution to be degraded was placed in this container.

The photocatalytic activities of the catalysts were determined by measuring the decrease in the concentration of *p*- nitroaniline and *m*- dinitrobenzoic acid with time in the reaction mixture. Prior to switching on the UV lamp, a suspension containing 0.2 gL^{-1} of the catalyst and 250 mL aqueous solution of ca. 50 ppm of the substrate was stirred continuously for 30 min in the dark for the adsorption of the compound on the surface of the catalyst. After the adsorption, the reaction mixture was irradiated and the samples were withdrawn using a syringe after every 10 min for first hour and then once every hour thereafter. The catalyst was separated from the samples by centrifugation before the analysis. The reaction mixture was kept homogeneous throughout by continuous stirring (ca. 500 rpm) the mixture using magnetic stirrer. The irradiation source was cooled by water circulation at 293 K during the experiments. The degradation of PNA (λ_{max} = 380) and DNBA (λ_{max} = 380) were determined by UV–Visible spectrophotometer (Cary 500, Varian Palo Alto CA). Total organic carbon content (TOC), to monitor the total mineralization of the substrates, was carried out by using total organic carbon analyzer (Liqui Toc, Elementar) equipped with IR detector. Separation of the catalyst particles before TOC analysis was done by filtering the sample solution using a 0.2μm Millipore membrane filter.

The liquid chromatography- mass spectroscopy (LC–MS) to determine the intermediates formed during the mineralization was performed on a *Q-Tof micro Y A-260 (Micromass, USA)* tandem quadruple-orthogonal Tof instrument, fitted with a lock spray source using Waters Mass Lynx Version 4.0 software. High performance liquid chromatography (HPLC) analysis was carried out by using an auto injector, a C-18 column 3.5 μm symmetry (2.1 x 100 mm column), a gradient made by two high pressure pumps (quaternary gradient) and waters 2996 photodiode array UV-Vis detector. Acetonitrile – Water (80% and 20%) mixture was used as a mobile phase with a flow rate of 0.2 ml min^{-1} in every analysis.

Results and Discussion

Structural Properties. X-ray diffraction patterns of the synthesized and P25 catalysts are shown in Fig. 1. The anatase (80 %) was the main phase content ($2\theta = 25.3$) with 20% brookite ($2\theta = 30.8$) corresponding to the (121) plane of brookite phase in SG catalyst. Rutile phase was found to be absent in SG catalyst as there was no peak observed at $2\theta = 27.4$, corresponding to the rutile phase. Catalyst SC contains (82 %) anatase phase along with 18% rutile phase. The anatase crystallite sizes of SG and SC catalysts was calculated as 13 nm and 8 nm respectively, which were lower than that of P25 (25 nm). Percentage crystallinity of both the catalysts synthesized by sol-gel and solution combustion method was found to be 51 and 40 % respectively with reference to P25 Degussa sample.

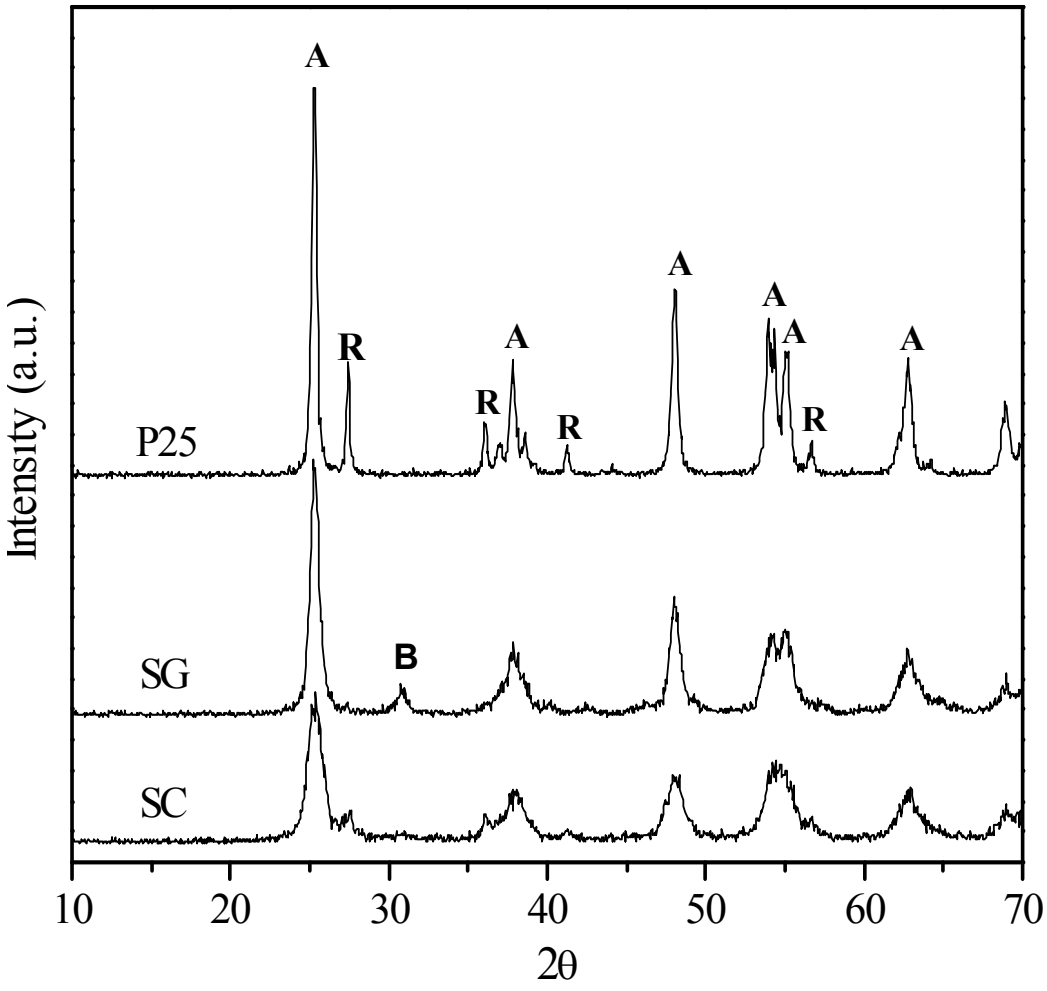

Fig. 1. X-ray diffraction pattern of synthesized and standard P-25 Degussa nanocrystalline titania catalysts (A = anatase, R = rutile, B = brookite).

The full width at half-maximum (FWHM) of the diffraction peak is related to the size of the nanomaterials [27] as narrower the peak larger will be the crystallite size. The reinforcement of diffraction of the X-ray beam because of the periodicity of the individual crystallite domains leads to a tall narrow peak. If the crystals are randomly arranged or have low degrees of periodicity, it results into a broader peak. The broadened peak of SC shows the lowest crystallinity among the catalysts studied (Fig. 1).

Nitrogen sorption isotherms (Fig. 2.) obtained for the two synthesized catalysts are of type IV (BDDT classification) [28] and have hysteresis loops. Type H2 hysteresis loops were obtained at low relative pressure between 0.4 and 0.7 which normally is observed in the case of pores with narrow necks wider bodies (ink bottle pores). Type H3 hysteresis loops were observed at high relative pressure between 0.8 and 1.0, often found with aggregates of plate like particles giving rise to slit like pores [21]. Pore size distribution curves of SG and SC are shown in the inset of Fig. 2. It is clear from the figure that there are different types of pores in SG with their diameter in the range of 5-11 nm and maximum pores having a diameter of 8 nm. While in SC, this range is narrow about 3-6 nm where the average pore diameter is 4 nm. TiO_2 synthesized through solution combustion method (SC) showed the highest surface area of 95 m^2/g. The surface area of the catalyst synthesized by sol-gel method was 80 m^2/g. Both the synthesized catalysts showed higher surface areas than P25 sample which was 54 m^2/g. Higher surface areas observed for the synthesized samples compared to P25 could be due to lower crystallinity as evidenced by X-ray diffraction.

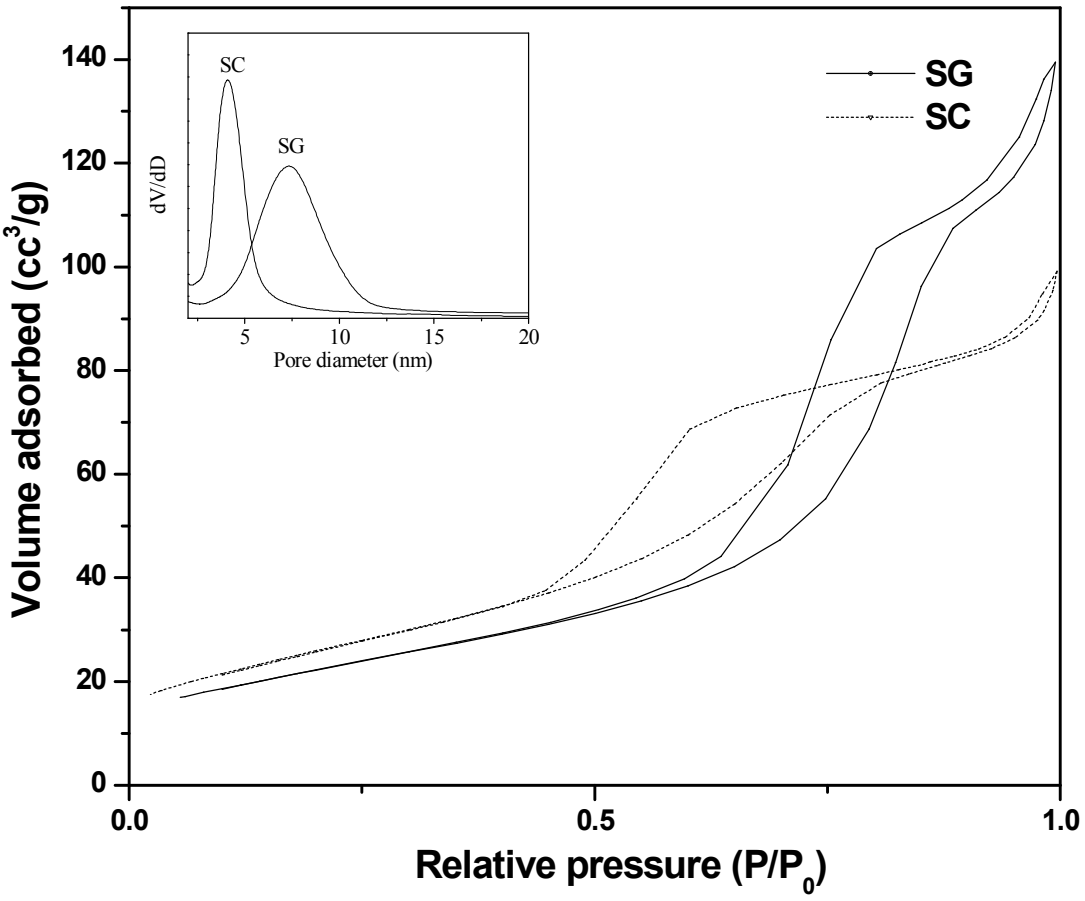

Fig. 2. N_2 adsorption/desorption isotherm of synthesized nanocrystalline titania catalysts.

The FT-IR spectra of all the catalysts are given in Fig 3. The fundamental vibrations of TiO_2 nanocrystals appear in IR-spectra as very intense broad bands, which were ascribed to the stretching vibrations of Ti-O bonds (550-680 cm^{-1}) and Ti-O-Ti bonds (436-495 cm^{-1}). Broad IR band at 3400-3437 cm^{-1} range is characterized by stretching –OH groups. IR band at 1020 cm^{-1} which was observed in P25 and SG is attributed to the Ti-OH deformation vibrations [29]. Literature contains a large amount of data on IR-spectral regions of deformation vibrations of adsorbed water molecules (~ 1620 cm^{-1}) and was observed in all catalysts at 1622-1630 cm^{-1} range [29]. Intense band at 1020 cm^{-1} in P25 indicates the presence of higher amount of surface hydroxyl groups than in other synthesized TiO_2 catalysts.

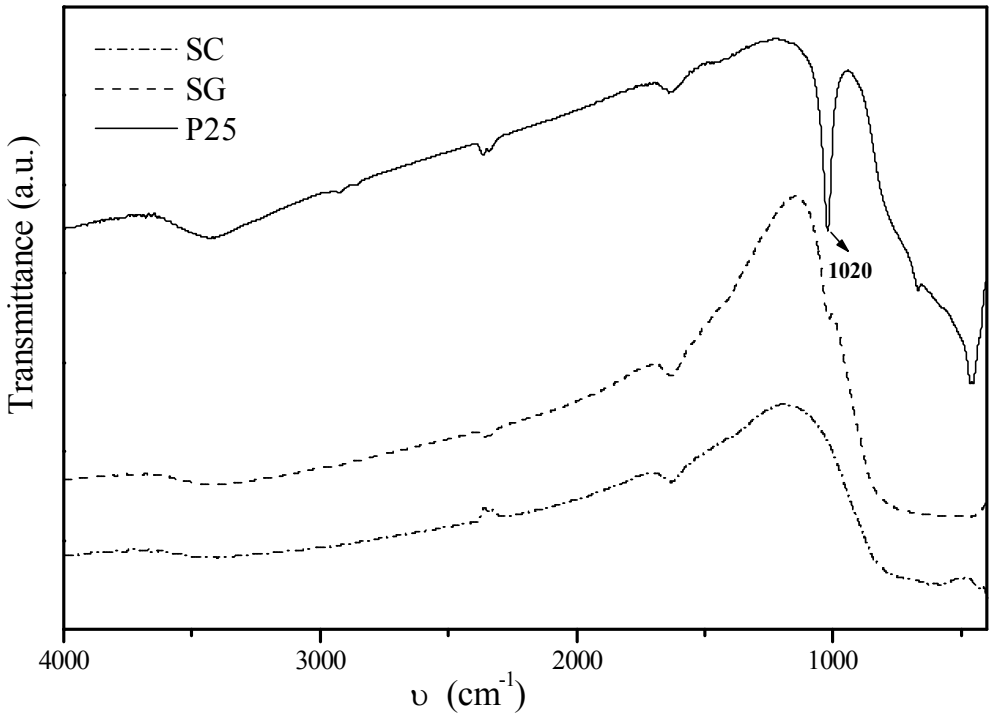

Fig. 3. FT-IR spectra of synthesized and standard P-25 Degussa nanocrystalline titania catalysts.

FT-Raman spectra's of the two synthesized catalysts is shown in Fig. 4. All the six Raman-active fundamentals [30], three E_g modes centered around 144, 197, and 637 cm^{-1}, two B_{1g} modes at 397 and 517 cm^{-1} and one A_{1g} mode at 513 cm^{-1}, in the vibrational spectrum of the anatase TiO_2 were observed. Besides, a peak at around 444 cm^{-1} was present in the spectrum of SC corresponding to rutile phase of TiO_2. It has been reported [30] that the most intense Eg (1) mode shows the blue shift and significant broadening with decrease in both crystallite size and crystallinity [31]. The observation is in agreement with the XRD results that SC has lowest crystallinity which leads toward in the broadening of Eg (1) mode with slight blue shift as compared to SG.

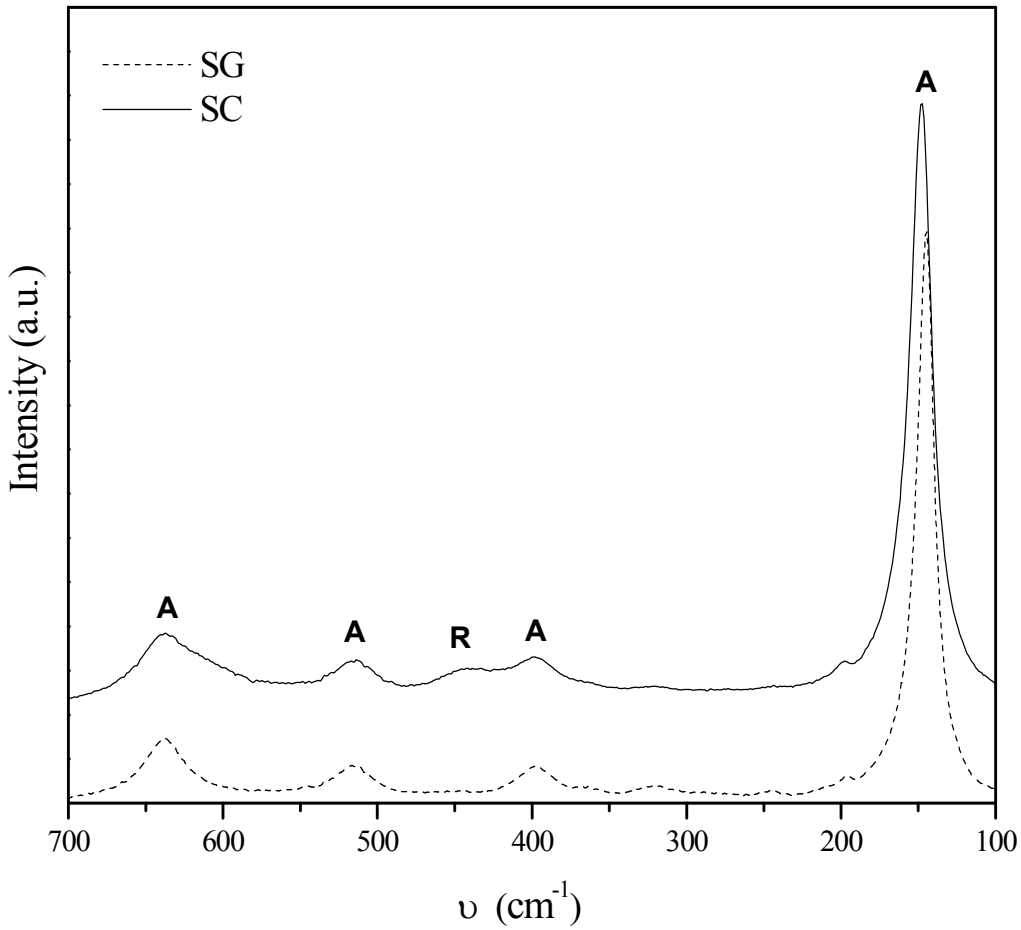

Fig. 4. FT-Raman spectra of synthesized nanocrystalline titania catalysts (A = anatase, R = rutile).

The band gap of synthesized catalysts was determined by UV-Vis diffuse reflectance spectroscopy. Bandgap values of SG and SC catalyst was calculated from DRS spectra were found to be 3.25 and 3.18 eV respectively. The different band gap values could be resulting from the difference in the surface microstructures, compositions and phase structures of the TiO_2 powders [32].

Thermo Gravimetric Analysis (TGA) results of SG and SC are shown in Fig. 5. There was only 1-2.5 % weight loss up to 800 °C. Major weight loss was observed up to 250 °C which is attributed to the removal of adsorbed water molecules. But in the case of SC sample, slight reduction in weight was noticed beyond 250 °C which could be due the removal of impurities apparently incorporated during synthesis.

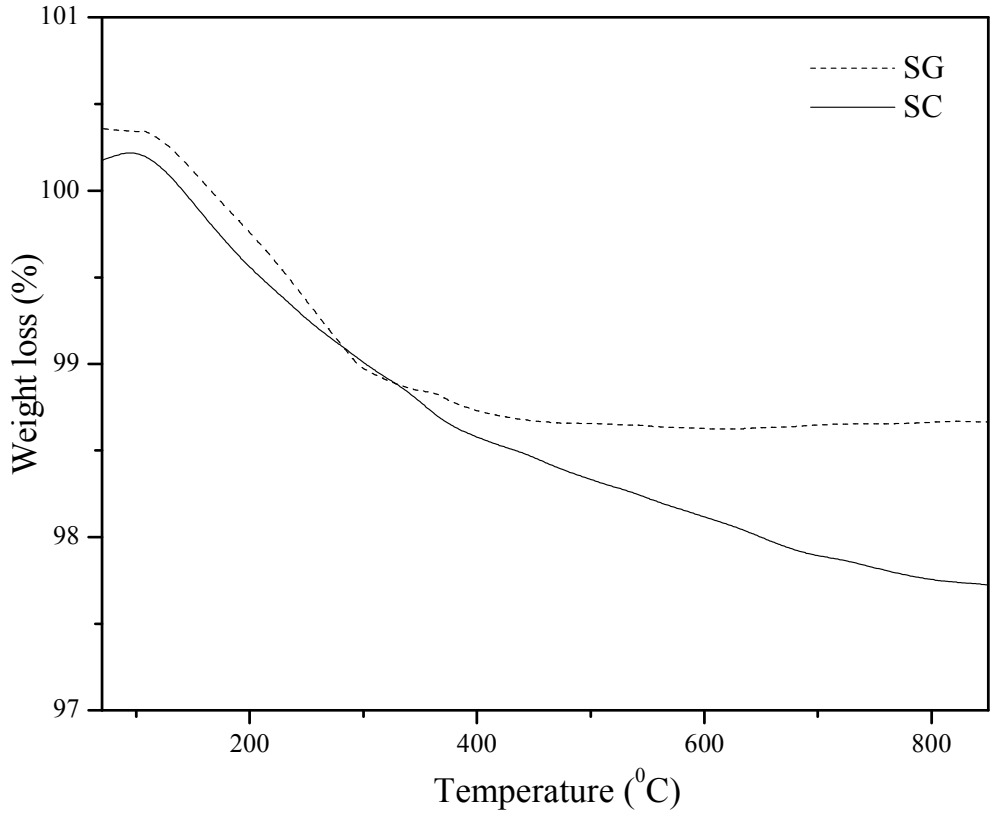

Fig. 5. TGA plot of synthesized nanocrystalline titania catalysts.

TEM images of the SG and SC catalysts [Fig.6] showed that these catalysts are spherical in shape. Crystallite size of SG and SC observed from TEM analysis was 11.5 and 7 nm respectively which are in agreement with the values obtained from X-ray diffraction analysis. The determination of OH-group (OH) concentration was carried out using NH_3-TPD experiment. The result showed that the OH group concentration was was in the range of SG>SC>P25 and it was 0.16299, 0.16706 and 0.05236 mmol g^{-1} for SC, SG and P25 catalysts respectively.

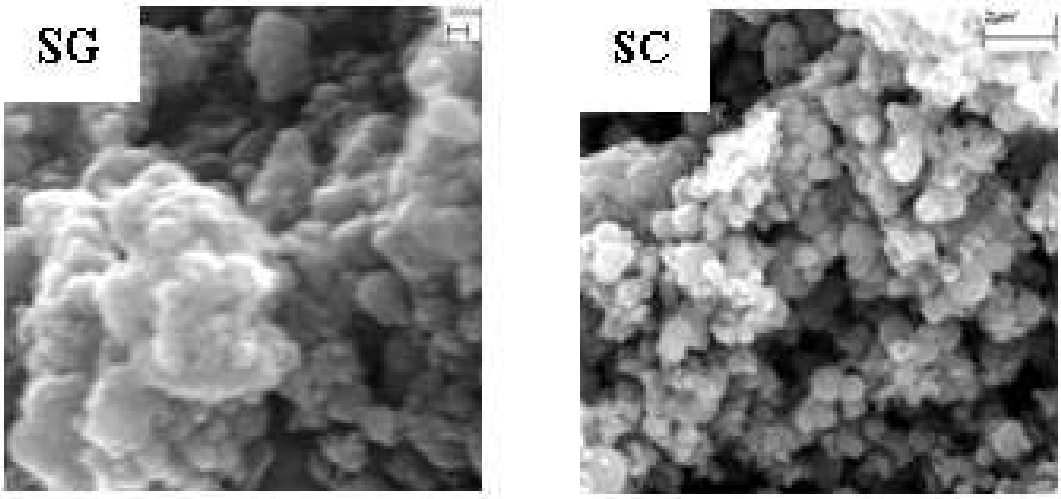

A) SEM images of SG and SC

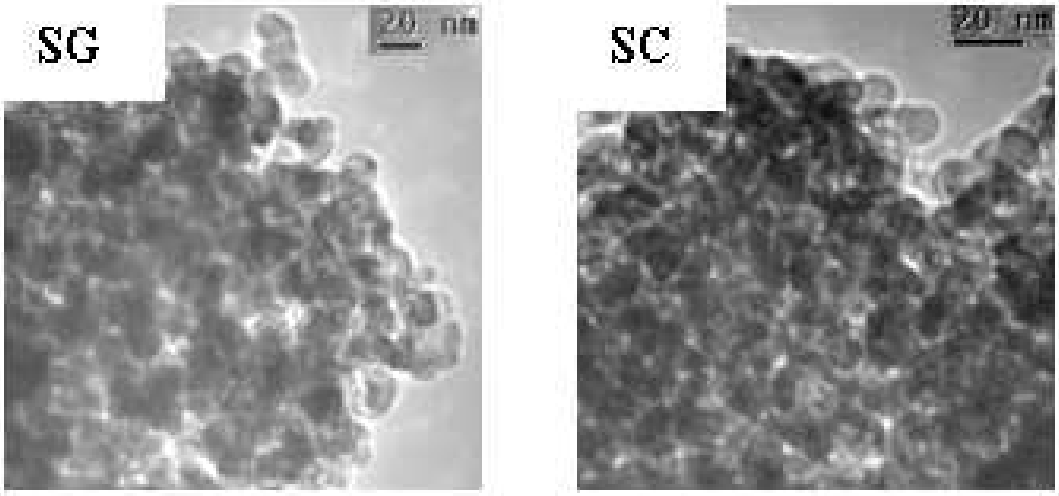

B) TEM images of SG and SC

Fig. 6. (A) SEM and (B) TEM images of SG, and SC.

Photocatalytic Degradation. The adsorption capacity of the all the catalysts could not de determined before under dark as it was found difficult to get separated from the reaction mixture and solution found turbid after centrifugation, whereas after photocatalytic experiments the catalysts was separated using centrifuge from PNA and DBNA reaction mixture. SC catalysts could not be determined as it was observed that the catalysts could not settle before the photocatalytic

experiments. Results of the photocatalytic experiments conducted are summarized in Table 1. All three different samples of TiO_2 photocatalyst (SG, SC and P25) were found to be efficient for the removal of both PNA and DNBA in aqueous solution. PNA showed 77-89 % decrease in concentration, measured from the UV-Vis absorbance data and indicated in the text as degradation, and it was 83-92 % for DNBA with different samples of TiO_2 catalysts after 4 hours of UV light exposure. The photocatalytic activity of the catalysts for the degradation of PNA and DNBA was observed in the order of SG > P-25 ≈ SC and SC > SG > P-25 respectively.

Table 1. Kinetics of the degradation of nitroaromatics.

Catalyst	*p*- nitroaniline				*m*- dinitrobenzoic acid			
	A	B	C	D	A	B	C	D
P25	77	5.0	1.3	70	83	3.6	1.3	79
SG	89	5.7	1.4	59	87	2.8	1.2	77
SC	79	4.6	1.2	44	92	2.3	1.1	71
NC	30	-	-	00	05	-	-	00

A: Percentage degradation, after 4 hours of UV light irradiation, determined by UV-Vis spectrophotometer

B: Initial Rate of degradation calculated using UV-visible absorbance data ($\times 10^6$ mol min^{-1})

C: Rate Constant calculated using UV-visible absorbance data ($k \times 10^2 min^{-1}$)

D: Percentage TOC removal after 4 hours of UV light irradiation (Initial TOC values for PNA= 26 mg/ L, DNBA= 24 mg/ L,)

NC: No catalysts (blank run)

The initial rate and rate constant from UV-vis analysis data for the degradation of PNA and DNBA were determined as pseudo first-order reaction kinetics and are given in Table 1. The initial rate of degradation with different catalysts was in the order of SG > P-25 > SC and P-25 > SG > SC for PNA and DNBA respectively.

The decrease in the total organic carbon (TOC), indicated as mineralization in the text, of PNA and DNBA was slower than the degradation process which is as expected. Mineralization is a slow process which usually passes through the formation of lot of intermediates before finally getting converted into CO_2, H_2O and other inorganic ions. Here PNA showed 44-70 % reduction in TOC and it was71-79 % for DNBA, by using different TiO_2 samples after 4 hours of UV light incidence. The efficiency of mineralization of different TiO_2 photocatalyst samples towards both PNA and DNBA followed in the order P-25 > SG > SC. A plausible mechanism for the mineralization of both PNA and DNBA, based on the results obtained from HPLC and LC-MS analyses is given in Scheme I and II.

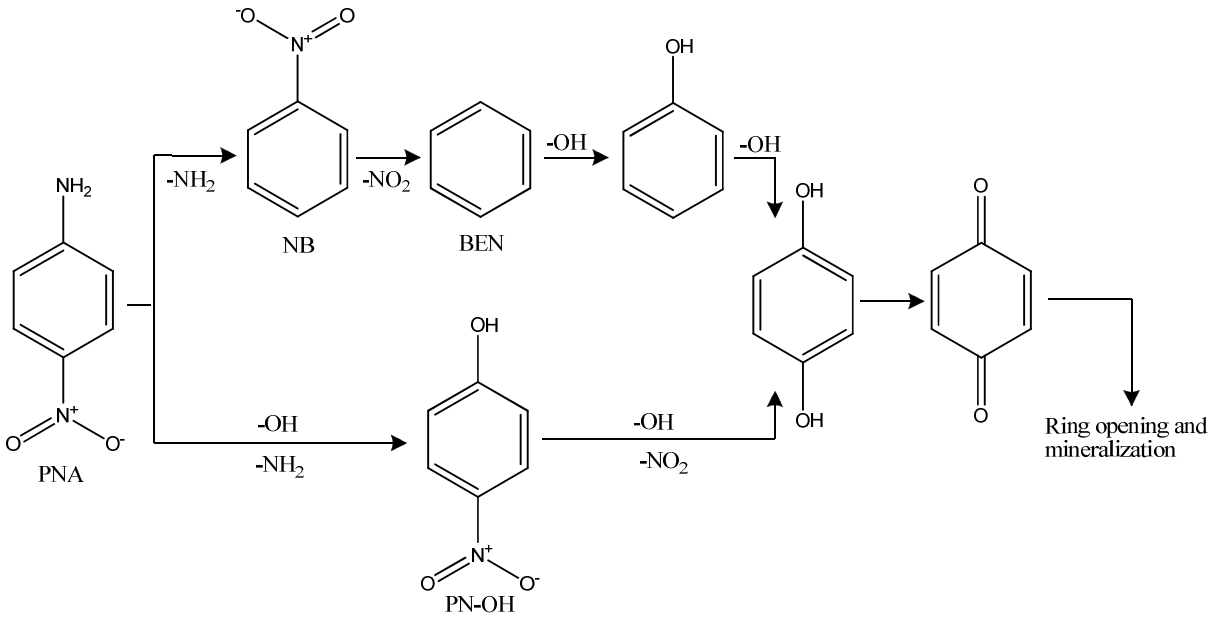

Scheme I. Proposed mineralization route for PNA.

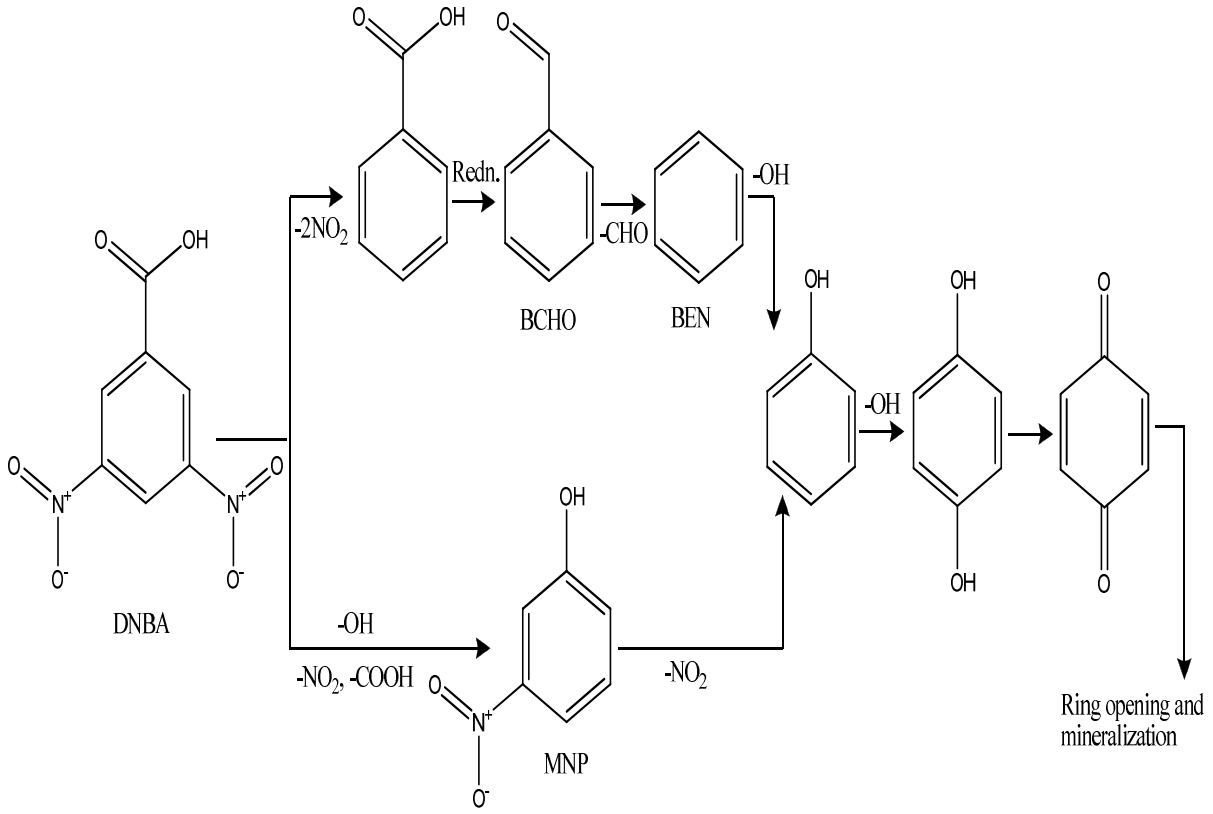

Scheme II. Proposed mineralization route for DNBA.

When experiments were conducted only in the presence of UV light, without TiO_2 catalyst (NC), PNA and DNBA showed 30 % and 5% decrease respectively in their concentration after 4 hours. However there wasn't any reduction in the TOC value of these samples even after 4 hours emphasizing the efficiency of TiO_2 as a photocatalyst.

The results demonstrated that the catalytic activity of the synthesized photocatalysts was different due the difference in their surface area, crystallinity, phase composition, band gap and surface hydroxyl content present in it. Among the three TiO_2 photocatalyst samples studied P25 was dominated over SG and SC for the mineralization of both PNA and DNBA. This could be attributed to its higher crystallinity (from XRD results Fig. 1), and slightly lower band gap (from DRS analysis) than SG and SC. It has been reported that the photocatalytic efficiency of amorphous TiO_2 is negligible indicating that crystallinity is one of the important requirements for TiO_2 to be an active photocatalyst [33]. Lower band gap could help P25 to absorb more radiations from the incident light

which might be able to enhance the electron-hole pair generation. It is recognized that a composite of anatase and rutile phases is beneficial for suppressing the recombination of photogenerated electrons and holes and by this means enhancing photocatalytic activity [34-36].

A large surface area can be determining factor in certain photocatalytic degradation reactions, as large amount of adsorbed organic molecules promotes the reaction rate [37, 38]. However, powders with large surface area are usually associated with large amounts of crystal defects, which favor the recombination of electrons and holes leading to a lower mineralizing activity [6]. That could be the reason why SG and SC with higher surface area (80 and 95 m^2/g respectively) than P25 (54 m^2/g) showed lower mineralizing activity.

Conclusion

TiO_2 photocatalyst syntheses by Sol-gel and solution combustion methods produces nanocrystalline TiO_2 with difference in phase contents, crystallinity, crystallite size, surface area, and band gap. Total mineralization of both PNA and DNBA was higher when P25 Degussa TiO_2 was used as the photocatalyst followed by SG and SC. Higher crystallinity and combination of anatase rutile phase of P25 over the synthesised catalysts are accountable for the greater mineralising power of P25 Degussa TiO_2 photocatalyst. Hence, the methods which can produce nanocrystalline TiO_2 with high crystallanity, low bandgap and higher surface area, along with other advantages, are preferable.

Acknowledgment

The authors are thankful to the Council of Scientific and Industrial Research, New Delhi, for the financial assistance under network project NWP 044. The authors are also thankful to Mr. C. K. Chandrakanth, Dr. Pragnya Bhatt, Mr. Vinod Agrawal, Mr. K. P. Prashanth, and Mr. Renjith Pillai for analytical support.

References

[1] A. Fujishima, K. Honda, Electrochemical photolysis of water at a semiconductor electrode, Nature (London) 238 (1972) 37-38.

[2] X. Chen, S.S. Mao, Titanium dioxide nanomaterials: Synthesis, properties, modifications and applications, Chem. Rev. 107 (2007) 2891-2959.

[3] A.L. Pruden, D.F. Ollis, Photoassisted heterogeneous catalysis: The degradation of trichloroethylene in water, J. Catal. 82 (1983) 404-417.

[4] C. Y. Hsiao, C. L. Lee, D. F. Ollis, Heterogeneous photocatalysis: Degradation of dilute solutions of dichloromethane (CH_2Cl_2), chloroform ($CHCl_3$), and carbon tetrachloride (CCl_4) with illuminated TiO_2 photocatalyst, J. Catal. 82 (1983) 418-423.

[5] A. Mills, S. L. Hunte, An overview of semiconductor photocatalysis, J. Photochem. Photobiol. A. 108 (1997) 1-35.

[6] D. Beydoun, R. Amal, G. Low, S. McEvoy, Role of nanoparticles in photocatalysis, J. Nanopart. Res. 1 (1999) 439-458.

[7] Y. Bessekhouad, D. Robert, J. V. Weber, Synthesis of photocatalytic TiO_2 nanoparticles: Optimization of the preparation conditions, J. Photochem. Photobiol. A Chem. 157 (2003) 47-53.

[8] K. Nagaveni, G. Sivalingam, M. S. Hegde, G. Madras, Solar photocatalytic degradation of dyes: High activity of combustion synthesized nano TiO_2, Appl. Catal. B. 48 (2004) 83-93.

[9] K. D. Kim, H. T. Kim, Synthesis of titanium dioxide nanoparticles using a continuous reaction method, Colloids and Surfaces A: Physicochem. Eng. Aspects 207 (2002) 263-269.

[10] Y. Li, T.J. White, S.H. Lim, Low-temperature synthesis and microstructural control of titania nano-particles, J. Solid State Chem. 177 (2004) 1372-1381.

[11] L. Znaidi, R. Seraphimova, J.F. Bocquet, C. Colbeau-Justin, C. Pommier, A semi-continuous process for the synthesis of nanosize TiO_2 powders and their use as photocatalysts, Mater. Res. Bull. 36 (2001) 811-825.

[12] D. Vorkapic, T. J. Matsoukas, Reversible agglomeration: A kinetic model for the peptization of titania nanocolloids, Colloid Interface Sci. 214 (1999) 283-291.

[13] G. Sivalingam, K. Nagaveni, M. S. Hegde, G. Madras, Photocatalytic degradation of various dyes by combustion synthesized nano anatase TiO_2, Appl. Catal. B. 45 (2003) 23-38.

[14] K. Nagaveni, G. Sivalingam, M. S. Hegde, G. Madras, Photocatalytic Degradation of Organic Compounds over Combustion-Synthesized Nano-TiO_2, Environ. Sci. Technol. 38 (2004)1600-1604.

[15] Agency for Toxic Substances and Disease Registry (ATSDR). Toxicological Profile for nitrobenzene; U.S. Department of Health and Human Services: Atlanta, GA, 1990. Public Health Service website: http:// www.atsdr.cdc.gov/taxfaq.html.

[16] A. C. Schmidt, R. Herzschuh, F. M. Matysik, W. Engewald, Investigation of the ionisation and fragmentation behaviour of different nitroaromatic compounds occurring as polar metabolites of explosives using electrospray ionisation tandem mass spectrometry, Rapid Commun. Mass Spectrom. 20 (2006) 2293-2302.

[17] A. C. Schmidt, B. Niehus, F. M. Matysik, W. Engewald, Identification and Quantification of Polar Nitroaromatic Compounds in Explosive-Contaminated Waters by means of HPLC-ESI-MS-MS and HPLC-UV, Chromatographia 63 (2006) 1-11.

[18] A. Bakdash, M. Ganswindt, S. Herre, T. Nadulski and F. Pragst, Lethal Poisoning with p-Nitroaniline, T + K 73 (2006) 61- 65.

[19] S. Gautam, S. P. Kamble, S. B. Sawant, V. G. Pangarkar, Photocatalytic degradation of 4-nitroaniline using solar and artificial UV radiation, Chem. Eng. J. 110 (2005) 129-137.

[20] H. Maa, M. Wanga, C. Pua, J. Zhanga, S. Zhaoa, S. Yaoa, J. Xiong, Transient and steady-state photolysis of p-nitroaniline in aqueous solution, J. Hazard. Mater. 165 (2009) 867-873.

[21] J. Yu, J. C. Yu, M. K-P. Leung, W. Ho, B. Cheng, X. Zhao, J. Zhao, Effects of acidic and basic hydrolysis catalysts on the photocatalytic activity and microstructures of bimodal mesoporous titania, J. Cata. 217 (2003) 69-78.

[22] J.G. Yu, J. F. Xiong, B. Cheng, S.W. Liu, Fabrication and characterization of Ag–TiO_2 multiphase nanocomposite thin films with enhanced photocatalytic activity, Appl. Catal. B. 60 (2005) 211-221.

[23] B. D. Cullity, S. R. Stock, Elements of X-ray Diffraction, third ed., Prentice Hall Inc. Upper Saddle River, NJ. 2001.

[24] S. J. Gregg, K. S. W. Sing, Adsorption, In Surface Area and Porosity, Academic Press, New York 1982.

[25] R. J. Tayade, R. G. Kulkarni, R. V. Jasra, Photocatalytic Degradation of Aqueous Nitrobenzene by Nanocrystalline TiO_2, Ind. Eng. Chem. Res. 45 (2006) 922-927.

[26] R. J. Tayade, R. G. Kulkarni, R.V. Jasra, Transition Metal Ion Impregnated Mesoporous TiO_2 for Photocatalytic Degradation of Organic Contaminants in Water, Ind. Eng. Chem. Res. 45 (2006) 5231-5238.

[27] M. Niederberger, M. H. Bartl, G. D. Stucky, Benzyl alcohol and titanium tetrachloride - A versatile reaction system for the nonaqueous and low-temperature preparation of crystalline and luminescent titania nanoparticles, *Chem. Mater.* 14 (2002) 4364-4370.

[28] K. S. W. Sing, D. H. Everett, R. A.W. Haul, L. Moscou, R. A. Pierotti, J. Rouquerol, T. Siemieniewska, Reporting Physisorption Data For Gas/Solid Systems with Special Reference to the Determination of Surface Area and Porosity, Pure Appl. Chem. 57 (1985) 603-619.

[29] T. Benzrondna, G. Puchkovska, V. Shyamanovska, J. Baran, H. Ratajczak, IR-analysis of h-bonded H_2O on the pure TiO_2 surface, J. Mol. Stru. 700 (2004) 175-181.

[30] V. Swamy, A. Kuznetsov, L. S. Dubrovinsky, R. A.Caruso, D. G. Shchukin, B. C. Muddle, Finite-size and pressure effects on the Raman spectrum of nanocrystalline anatase TiO_2, Phys. Rev.B. 71(18) (2005) 1-11.

[31] J. Zhu, J. Zhang, F. Chen , K. Iino, M. Anpo, High activity TiO_2 photocatalysts prepared by a modified sol-gel method: Characterization and their photocatalytic activity for the degradation of XRG and X-GL, Topics in Catalysis. 35 (2005) 261-268.

[32] J. Yu, H. Yu, B. Cheng, M. Zhou, X. Zhao, Enhanced photocatalytic activity of TiO2 powder (P25) by hydrothermal treatment, J. Mol. Cat. A. Chem. 253 (2006) 112-118.

[33] B. Ohtani, S. Ogawa, S. -I. Nishimoto, Photocatalytic activity of amorphous-anatase mixture of titanium (IV) oxide particles suspended in aqueous solutions, J. Phys. Chem. B. 101 (1997) 3746-3752.

[34] D. S. Bhatkhande, V. G. Pangarkar, A. A. Beenackers, Photocatalytic degradation of nitrobenzene using titanium dioxide and concentrated solar radiation: Chemical effects and scaleup, *Water Research* 37 (2003) 1223-1230.

[35] J. C. Yu, J. Yu, W. Ho, L. Zhang, Preparation of highly photocatalytic active nano-sized TiO_2 particles via ultrasonic irradiation, Chem. Commun. 19 (2001) 1942-1943.

[36] J. C. Yu, J. Yu, L. Zhang, W. Ho,_Enhancing effects of water content and ultrasonic irradiation on the photocatalytic activity of nano-sized TiO_2 powders, J. Photochem. Photobiol. A. 148 (2002) 263-271.

[37] K. H. Wang, Y. H. Hsieh, C. H. Wu, C. Y. Chang, The pH and anion effects on the heterogeneous photocatalytic degradation of o-methylbenzoic acid in TiO_2 aqueous suspension, Chemosphere 40 (2000) 389-394.

[38] C. Chen, K. Wang, L. Lou, Photodegradation of dye pollutants on silica gel supported TiO2 particles under visible light irradiation, J. Photo. Chem. Photo. Biol. A. 163 (2004) 281-287.